Localized and stationary light wave modes in dispersive media

Miguel A. Porras
Departamento de Física Aplicada, ETSIM, Universidad Politécnica de Madrid, Rios Rosas 21, 28003 Madrid, Spain

Paolo Di Trapani
INFM and Department of Chemical, Physical and Mathematical Sciences, University of Insubria, Via Valleggio 11, 22100 Como, Italy
(Received 10 September 2003; published 9 June 2004)

In recent experiments, localized and stationary optical wave packets have been generated in second-order nonlinear processes with femtosecond pulses, whose asymptotic features relate to those of nondiffracting and nondispersing polychromatic Bessel beams in linear dispersive media. We investigate the nature of these linear waves and show that they can be identified with the X-shaped (O-shaped) modes of the hyperbolic (elliptic) wave equation in media with normal (anomalous) dispersion. Depending on the relative strengths of mode phase mismatch, group velocity mismatch with respect to a plane pulse, and the defeated group velocity dispersion, these modes can adopt the form of pulsed Bessel beams, focus wave modes, and X waves (O waves), respectively.

DOI: 10.1103/PhysRevE.69.066606 PACS number(s): 42.65.Tg, 42.65.Re

I. INTRODUCTION

Stationary, temporally, and spatially localized, X-shaped optical wave packets, having a duration of a few tens of femtoseconds and spot size of a few microns, have been recently observed to be spontaneously generated in dispersive nonlinear materials from a standard laser wave packet [1–3]. Balancing between second-order or Kerr nonlinearity, group velocity dispersion, and angular dispersion and diffraction has been suggested to act as a kind of mode-locking mechanism that drives pulse reshaping and keeps the interacting waves trapped and phase and group matched [4–6].

The purpose of the present paper is to investigate the nature of these waves. The main hypothesis underlying our investigation is that these nonlinearly generated X-shaped waves behave asymptotically as linear waves. This assumption is based, first, on the observed stationarity, not only of the central hump of the wave packet, but also of its asymptotic, low-intensity, conical part [1–3], stationarity that cannot be attributed to nonlinear wave interactions, but to some linear mechanism of compensation between material and angular dispersion. Indeed, several kinds of linear polychromatic versions of Bessel beams [7], such as Bessel-X pulses [8,9], pulsed Bessel beams [10,11], subcycle Bessel-X pulses or focus wave modes [12], and envelope X waves [13], with the capability of maintaining transversal and temporal (longitudinal) localization in linear media with normal group velocity dispersion (GVD), have been described in recent years (for a unified description and an extension to media with anomalous dispersion, see also Ref. [14]). In contrast to free-space X waves [15] and Bessel-X pulses [16,17], stationarity in dispersive media requires the introduction of an appropriate amount of cone-angle dispersion that leads to the cancellation of material GVD with cone-angle dispersion-induced GVD [8–14]. Second, polychromatic Bessel beams, with or without angular dispersion [14], have the ability of propagating at rather arbitrary effective phase and group velocities in dispersive media, as has to be done by the phase-matched and mutually trapped fundamental [3] and second-harmonic [5] nonlinearly generated X waves.

For these reasons, in this paper we present a more comprehensive description of localized and stationary optical waves in linear dispersive media, henceforth called *wave modes*, which is particularly suitable for understanding and predicting the spatiotemporal features of the nonlinear X waves generated in experiments. From a linear point of view, this description allows us to predict the existence of new kinds of wave modes and classify all of them according to the values of a few physically meaningful parameters.

Each wave mode is specified by the values of the defeated material GVD, the mode group velocity mismatch (GVM), and phase mismatch (PM) with respect to a plane pulse of the same carrier frequency in the same medium. Wave modes are then shown (Sec. II) to belong to two broad categories: hyperbolic modes, with X-shaped spatiotemporal structure, if material dispersion is normal, or elliptic modes, with O-shaped structure, if material dispersion is anomalous [18]. In Sec. III we show that each wave mode can adopt the approximate form of (1) a pulsed Bessel beam (PBB), (2) an *envelope focus wave mode* (eFWM), or (3) an envelope X (eX) wave in normally dispersive media [*envelope O* (eO) *wave* in anomalously dispersive media], according to whether the mode bandwidth makes PM, GVM, or defeated GVD, respectively, to be the dominant mode characteristic of propagation. This classification allows us to understand the spatiotemporal features of wave modes in dispersive media in terms of a few parameters (the characteristic PM, GVM, and GVD lengths), including modes with mixed pulsed Bessel, focus wave mode, and X-like (O-like) structure.

The above description is obtained from the paraxial approximation to wave propagation. We choose this approach because of its wider use in nonlinear optics and because it leads to simpler expressions in terms of parameters directly linked to the physically relevant properties of the mode and dispersive medium. In Sec. IV we compare the paraxial and more exact nonparaxial approaches to show that the paraxial approach is accurate enough for the description of wave

modes currently generated by linear optical devices [9,10] and in nonlinear wave mixing processes [1–3].

II. WAVE MODES OF THE PARAXIAL WAVE EQUATION

We start by considering the propagation of a three-dimensional wave packet $E(\boldsymbol{x}_\perp,z,t)=A(\boldsymbol{x}_\perp,z,t)\exp(-i\omega_0 t+ik_0 z)[\boldsymbol{x}_\perp\equiv(x,y)]$ of a certain optical carrier frequency ω_0, subject to the effects of diffraction and dispersion of the material medium. Within the paraxial approximation and up to second order in dispersion, the propagation of narrow-band pulses is ruled by the equation

$$\partial_z A=\frac{i}{2k_0}\Delta_\perp A-i\frac{k_0''}{2}\partial_\tau^2 A, \tag{1}$$

where z is the propagation direction, $\tau=t-k_0' z$ is the local time, $\Delta_\perp\equiv\partial_x^2+\partial_y^2$, and $k_0^{(i)}\equiv\partial_\omega^{(i)}k(\omega)|_{\omega_0}$, with $k(\omega)$ the propagation constant in the medium. Equation (1) is valid for a narrow envelope spectrum $\hat{A}(\boldsymbol{x}_\perp,z,\Omega)$ around $\Omega\equiv\omega-\omega_0=0$ — that is, for bandwidths

$$\Delta\Omega\ll\omega_0, \tag{2}$$

a condition that requires at least few carrier oscillations to fall within the envelope A.

We search for stationary and localized solutions of Eq. (1) in the wide sense that the *intensity* does not depend on z in a reference frame moving at *some velocity*. These solutions must then be of the form

$$A(x,y,\tau,z)=\Phi(x,y,\tau+\alpha z)\exp(-i\beta z). \tag{3}$$

The free parameters α and β are assumed to be small in the sense that

$$|\alpha|\ll k_0', \tag{4}$$

$$|\beta|\ll k_0, \tag{5}$$

so that the group velocity $1/(k_0'-\alpha)$ and phase velocity $\omega_0/(k_0-\beta)$ of the wave differ slightly from those of a plane pulse of the same carrier frequency in the same material, $1/k_0'$ and ω_0/k_0, respectively.

Under the assumption of asymptotic linear behavior of nonlinear X waves, we can get some insight into the possible values of α and β of nonlinear X waves on the only basis of the linear dispersive properties of the medium. If, for instance, a pulse of frequency ω_F generates a stationary and localized second-harmonic pulse ($\omega_0=2\omega_F$) traveling at the same group and phase velocities as the fundamental pulse [5], we must have $k_0'-\alpha=k_F'$ and $k_0-\beta=2k_F$ —that is, $\alpha=k_F'-k_0'$ and $\beta=\Delta k\equiv k_0-2k_F$. For illustration, Fig. 1 shows the values of α and β of the second-harmonic pulse in lithium triborate (LBO) as a function of its carrier frequency ω_0. Note also that $|\alpha|$ and $|\beta|$ satisfy the conditions (4) and (5) for any carrier frequency in the entire visible range and beyond.

In Sec. IV, a nonparaxial approach to the problem stated above will be performed. It will be shown that the paraxial and nonparaxial descriptions yield substantially the same results if conditions (2), (4), and (5) are satisfied, as is the case of the experiments and numerical simulations demonstrating the spontaneous generation of X-type waves [1–3].

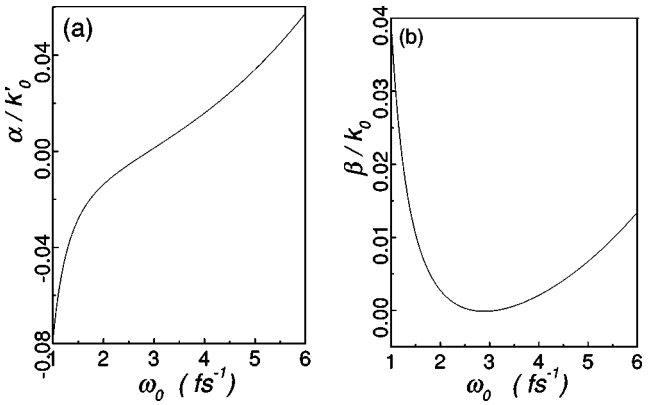

FIG. 1. Values of α and β of the localized and stationary, second-harmonic waves of different carrier frequencies ω_0 for phase and group matching with the fundamental wave in the process of oo-e second harmonic generation in LBO at room temperature. Dispersion formulas for the refraction index are taken from Ref. [19].

Equation (1) with ansatz (3) yields

$$\Delta_\perp\Phi-k_0k_0''\partial_\tau^2\Phi+2ik_0\alpha\partial_\tau\Phi+2k_0\beta\Phi=0, \tag{6}$$

as the differential equation for the reduced envelope Φ of the wave modes. Equation (6) is a hyperbolic differential equation in normally dispersive media and an elliptic differential equation in media with anomalous dispersion [20]. For the temporal spectrum $\hat{\Phi}(x,y,\Omega)$ of the reduced envelope $\Phi(x,y,\tau+\alpha z)$, Eq. (6) yields the Helmholtz-type equation $\Delta_\perp\hat{\Phi}+K^2(\Omega)\hat{\Phi}=0$, where

$$K(\Omega)=\sqrt{2k_0\left(\beta+\alpha\Omega+\frac{1}{2}k_0''\Omega^2\right)} \tag{7}$$

will be referred to as the (transversal) dispersion relation since it relates the modulus K of the transversal component of the wave vector with the detuning Ω of each monochromatic wave component from the carrier frequency ω_0. For Ω such that $K(\Omega)$ is real, the Helmholtz equation admits the bounded, cylindrically symmetric, Bessel-type solution $\hat{\Phi}(r,\Omega)=\hat{f}(\Omega)J_0[K(\Omega)r]$, where $\hat{f}(\Omega)$ is an arbitrary spectral amplitude and $J_0(\cdot)$ the Bessel function of zero order and first class [21]. By inverse Fourier transform we can write the expression

$$\Phi_{\alpha,\beta}(r,\tau+\alpha z)=\frac{1}{2\pi}\int_{K(\Omega)\text{real}}d\Omega\hat{f}(\Omega)J_0K[(\Omega)r]\times\exp[-i\Omega(\tau+\alpha z)] \tag{8}$$

for the reduced envelope of the cylindrically symmetric wave modes, or localized, propagation invariant solutions of the paraxial wave equation, in the sense explained above. As indicated, the integration domain extends over frequencies Ω such that the dispersion curve $K(\Omega)$ is real. According to Eq.

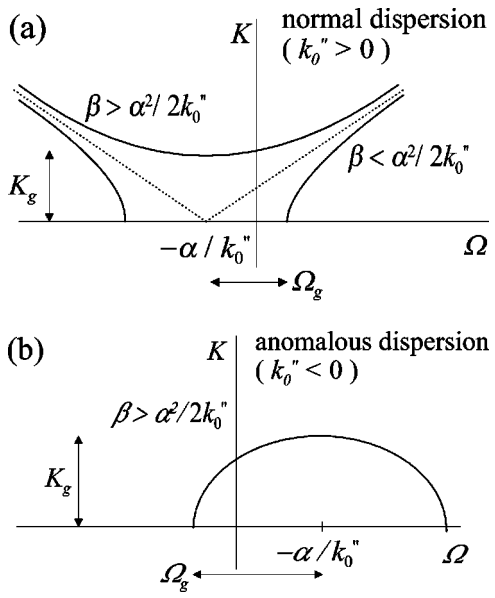

FIG. 2. Dispersion curve of the wave modes in a medium with (a) normal dispersion and (b) anomalous dispersion.

(8), a wave mode $\Phi_{\alpha,\beta}$ is composed of locked monochromatic Bessel beams whose frequencies and radial wave vectors are linked by a specific dispersion relation $K(\Omega)$ and whose relative weights are determined by a certain spectral amplitude $\hat{f}(\Omega)$.

As shown in Figs. 2(a) and 2(b), the form of the dispersion curve $K(\Omega)$ reflects the underlying hyperbolic or elliptic geometries of the differential equation (6) for wave modes in the respective cases of propagation in media with normal or anomalous dispersion. For normal dispersion ($k_0''>0$), $K(\Omega)$ is in fact a single-branch vertical hyperbola if $\beta>\alpha^2/2k_0''$ and a two-branch horizontal hyperbola if $\beta<\alpha^2/2k_0''$ [see Fig. 2(a)]. For anomalous dispersion ($k_0''<0$), $K(\Omega)$ takes real values only if $\beta>\alpha^2/2k_0''$, in which case the dispersion curve is an ellipse [see Fig. 2(b)]. It is also convenient to introduce the (real or imaginary) frequency gap

$$\Omega_g \equiv \sqrt{\frac{\alpha^2}{k_0''^2}-\frac{2\beta}{k_0''}} \tag{9}$$

and radial wave vector gap

$$K_g \equiv \sqrt{-k_0 k_0'' \Omega_g^2}. \tag{10}$$

When Ω_g and K_g are real, they represent actual frequency and radial wave vector gaps in the dispersion curve $K(\Omega)$, as illustrated in Fig. 2. In any case, their moduli characterize the scales of variation of the frequency and radial wave vector in the dispersion curves.

Closely connected with the dispersion curve are the so-called *impulse response* wave modes $\Phi^{(i)}_{\alpha,\beta}(r,\tau+\alpha z)$ or modes with $\hat{f}(\Omega)=1$. As seen in Fig. 3, the structure of $\Phi^{(i)}_{\alpha,\beta}$ in space and time closely resembles that of the dispersion curve in the K-Ω plane and, hence, the hyperbolic or elliptic nature of the differential equation for wave modes [20], but at radial and temporal scales of variation characterized by the reciprocal quantities $|K_g|^{-1}$ and $|\Omega_g|^{-1}$, respectively. Equation (8) with $\hat{f}(\Omega)=1$ and the change $\Omega'=\Omega+\alpha/k_0''$ yields

$$\Phi^{(i)}_{\alpha,\beta}(r,z,\tau)=\frac{1}{2\pi}\int_{K(\Omega')\text{real}} d\Omega' J_0[K(\Omega')r] \times\exp[-i\Omega'(\tau+\alpha z)]\exp\left[i\frac{\alpha}{k_0''}(\tau+\alpha z)\right], \tag{11}$$

where

$$K(\Omega')=\sqrt{k k_0''\left(\Omega'^2+\frac{2\beta}{k_0''}-\frac{\alpha^2}{k_0''^2}\right)}. \tag{12}$$

The integral in Eq. (11) can be performed in all possible cases from formulas 6.677.3 (for $k_0''>0$, $\beta>\alpha^2/2k_0''$), 6.677.2 (for $k_0''>0$, $\beta<\alpha^2/2k_0''$), and 6.677.6 (for $k_0''<0$, $\beta>\alpha^2/2k_0''$) of Ref. [21], to yield the closed-form expression for impulse response modes,

$$\Phi^{(i)}_{\alpha,\beta}(r,\tau+\alpha z) =\frac{1}{2\pi}\left[\frac{1}{\sqrt{k_0 k_0'' r^2-(\tau+\alpha z)^2}}\exp \times\left\{i\left[\sqrt{\frac{2\beta}{k_0''}-\frac{\alpha^2}{k_0''^2}}\sqrt{k_0 k_0'' r^2-(\tau+\alpha z)^2}\right]\right\}+\text{c.c.}\right] \times\exp\left[\frac{i\alpha}{k_0''}(\tau+\alpha z)\right] \tag{13}$$

or, in terms of the frequency and radial wave vector gaps,

$$\Phi^{(i)}_{\alpha,\beta}=\frac{1}{2\pi}\left[\Omega_g\frac{\exp(iR)}{iR}+\text{c.c.}\right]\exp\left[\frac{i\alpha}{k_0''}(\tau+\alpha z)\right], \tag{14}$$

where $R=[K_g^2 r^2+\Omega_g^2(\tau+\alpha z)^2]^{1/2}$.

As shown in Fig. 3(a), for $k_0''>0$ and $\beta>\alpha^2/2k_0''$ (Ω_g imaginary and K_g real), the impulse response wave mode is singular in the cone $r=|(\tau+\alpha z)|/\sqrt{k_0 k_0''}$, is zero for $r<|(\tau+\alpha z)|/\sqrt{k_0 k_0''}$ (within the cone), and decays as $1/r$ for $r>|(\tau+\alpha z)|/\sqrt{k_0 k_0''}$ (out of the cone). The radial beatings in this region, of period $2\pi/K_g$, are a consequence of the radial wave vector gap K_g.

Figure 3(b) shows the impulse response mode for $k_0''>0$ and $\beta<\alpha^2/2k_0''$ (Ω_g real and K_g imaginary). As in the previous case, the mode is singular at the cone $r=|(\tau+\alpha z)|/\sqrt{k_0 k_0''}$, but damped oscillations are now temporal, of period $2\pi/\Omega_g$, as corresponds to the frequency gap Ω_g in the dispersion curve. Out of the cone $[r>|(\tau+\alpha z)|/\sqrt{k_0 k_0''}]$ the mode is exponentially localized.

Modes in media with anomalous dispersion— i.e., with $k_0''<0$ and $\beta>\alpha^2/2k_0''$ (real Ω_g and K_g) — exhibit rather different characteristics [Fig. 3(c)]. These modes are no longer singular and of X type, but regular and, say, of O type. The damped oscillations decay temporally and radially as $1/t$ and $1/r$, respectively, with periods $2\pi/\Omega_g$ and $2\pi/K_g$. The

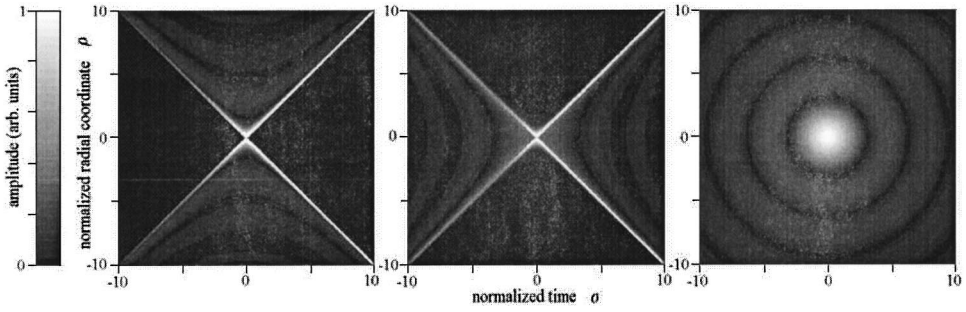

FIG. 3. Gray-scale plot of the amplitude $|\Phi^{(i)}_{\alpha,\beta}|$ of the impulse response wave modes. (a) Normal dispersion $k_0''>0$ with $\beta>\alpha^2/2k_0''$ (Ω_g imaginary, transversal wave vector gap K_g real). (b) Normal dispersion $k_0''>0$ with $\beta<\alpha^2/2k_0''$ (detuning gap Ω_g real, K_g imaginary). (c) Anomalous dispersion $k_0''<0$ with $\beta>\alpha^2/2k_0''$ (Ω_g and K_g real). Normalized local time and radial coordinate are defined as $\sigma=|\Omega_g|(\tau+\alpha z)$ and $\rho=|K_g|r$, respectively

absence of singularities is a consequence of the actual limitation that the elliptic dispersion curve imposes to the uniform spectrum $\hat{f}(\Omega)=1$.

III. CLASSIFICATION OF WAVE MODES

Numerical integration of Eq. (8) with a given dispersion curve (specified by the values of α, β, and k_0'') but different (bell-shaped) spectral amplitude functions $\hat{f}(\Omega)$, having also different (but finite) bandwidths $\Delta\Omega$ [alternatively, numerical integration of

$$\Phi_{\alpha,\beta}(r,\tau+\alpha z)=\int_{-\infty}^{\infty}d\sigma\Phi^{(i)}_{\alpha,\beta}(r,\tau+\alpha z-\sigma) \tag{15}$$

where $f(\tau)$ is the inverse Fourier transform of $\hat{f}(\Omega)$], shows much richer and complex spatiotemporal features in comparison with the case of infinite bandwidth. These features strongly depend on the choice of the spectral bandwidth $\Delta\Omega$, while no essentially new properties arise from the specific choice of $\hat{f}(\Omega)$ (Gaussian, Lorentzial, two-side exponential, etc.). Modes with finite bandwidth may exhibit mixed, more or less pronounced radial and temporal oscillations, along with incipient or strong X-wave (O-wave), focus wave mode, or Bessel structure, as explained throughout this section (see also the following figures). The purpose of this section is to perform a simple, comprehensive classification of wave modes in dispersive media. In the remainder of this paper, $\Delta\Omega$ will refer to any suitable definition of the half-width of the bell-shaped spectral amplitude function $\hat{f}(\Omega)$.

Given a mode of parameters α and β satisfying conditions (4) and (5), propagating in a dispersive material with GVD k_0'', and some spectral bandwidth $\Delta\Omega$ satisfying Eq. (2), we have found it convenient to define the three following characteristic lengths: (1) the mode PM length

$$L_p\equiv\frac{1}{\beta}, \tag{16}$$

(2) the mode walk-off or GVM length

$$L_w\equiv\frac{1}{\alpha\Delta\Omega}, \tag{17}$$

measuring, respectively, the axial distances at which the mode becomes phase mismatched and walks off *with respect to a plane pulse of the same spectrum in the same medium*, and (3) the GVD length

$$L_d\equiv\frac{1}{k_0''(\Delta\Omega)^2}, \tag{18}$$

or distance at which the mode (invariable) duration differs significantly from that of the (broadening) plane pulse. Note that, as defined, L_p, L_w, and L_d can be positive or negative. In terms of the mode lengths the transversal dispersion relation (7) takes the form

$$K(\Omega)=\sqrt{2k_0\left(L_p^{-1}+L_w^{-1}\Omega_n+\frac{1}{2}L_d^{-1}\Omega_n^2\right)}, \tag{19}$$

where $\Omega_n=\Omega/\Delta\Omega$ is the normalized detuning, which ranges in $[-1,+1]$ for Ω within the bandwidth $\Delta\Omega$. Then, they are the values of the mode lengths L_p, L_w, and L_d that determine the form of the dispersion curve within the spectral bandwidth and, hence, the parameters that determine the spatiotemporal structure of the mode, as shown throughout this section. We analyze here three extreme cases— namely,

$$|L_p|\ll|L_w|,|L_d| \quad \text{PM - dominated case},$$

$$|L_w|\ll|L_p|,|L_d| \quad \text{GVM - dominated case},$$

$$|L_d|\ll|L_p|,|L_w| \quad \text{GVD - dominated case},$$

which represent three well-defined, opposite experimental situations and which allow us also to understand, at least qualitatively, the features of general, intermediate cases.

For illustration, we have evaluated the characteristic lengths of wave modes of different frequencies ω_0 that propagate in LBO at the phase and group velocities of the corresponding fundamental waves of half-frequency. In Fig. 4, the bandwidths $\Delta\Omega=\omega_0/2\pi N$ correspond to "N-cycle" pulses [duration $\sim(\Delta\Omega)^{-1}=NT_0$, $T_0=2\pi/\omega_0$ period] at each frequency ω_0. The value $N=10$ in Fig. 4(a) leads to a pulse

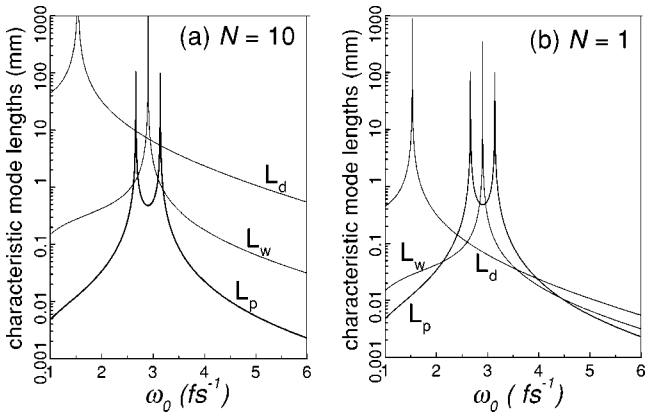

FIG. 4. Characteristic lengths of extraordinary second-harmonic wave modes of different frequencies in the visible range that travel at the phase and group velocities of the ordinary fundamental waves in LBO at room temperature. Mode bandwidths are $\Delta\Omega/\omega_0 = 1/2\pi N$, with (a) $N=10$ and (b) $N=1$.

duration $(\Delta\Omega)^{-1}\sim 20$ fs at $\omega_0 = 3.55$ fs^{-1}($\lambda = 0.53$ μm), of the same order as in previous experiments and numerical simulations. Figure 4(b) shows, in contrast, the extreme case of "single-cycle" wave modes. Generally speaking, modes of long enough duration belong to, or participate mostly in, the PM-dominated case [as in Fig. 4(a) for most frequencies], modes of some (still unspecified) intermediate duration belong to the GVM-dominated case, and extremely short modes to the GVD-dominated case, since L_p is independent of bandwidth, but L_p and L_d are inversely proportional to $\Delta\Omega$ and $\Delta\Omega^2$, respectively. Depending, however, on the relative values of α, β, and k_0'' (particularly when one or two of them are very small), the GVM-dominated case, even the PM-dominated case, can extend down to the single-cycle regime [as in Fig. 4(b) for most frequencies] or, on the contrary, the GVM-dominated case, even the GVD-dominated case, apply to considerably long modes [as in the vicinity of the two singularities of the L_p curve of Fig. 4(a)].

A. Phase-mismatch-dominated case: Pulsed Bessel-beam-type modes

Consider first modes with $|L_p| \ll |L_w|, |L_d|$. When $L_p > 0$, the dispersion curve within the spectral bandwidth can be approached by the real constant value $K(\Omega) \simeq (2k_0 L_p^{-1})^{1/2}$ or

$$K(\Omega) \simeq \sqrt{2k_0\beta} \quad (\text{if } \beta > 0) \tag{20}$$

[see Fig. 5(a)], regardless the exact dispersion curve is an actual hyperbola or ellipse [as in Fig. 5(b)]— that is, independently of the sign of material group velocity dispersion. Wave modes under these conditions can only have superluminal phase velocity ($\beta > 0$), but superluminal or subluminal group velocity ($\alpha > 0$ or $\alpha < 0$, respectively), and will adopt, from Eqs. (8) and (20), the approximate factorized form

$$\Phi_{\alpha,\beta}(r, \tau + \alpha z) \simeq f(\tau + \alpha z) J_0(\sqrt{2k_0\beta}\, r) \tag{21}$$

of a PBB of transversal size of the order of $(2k_0\beta)^{-1/2}$.

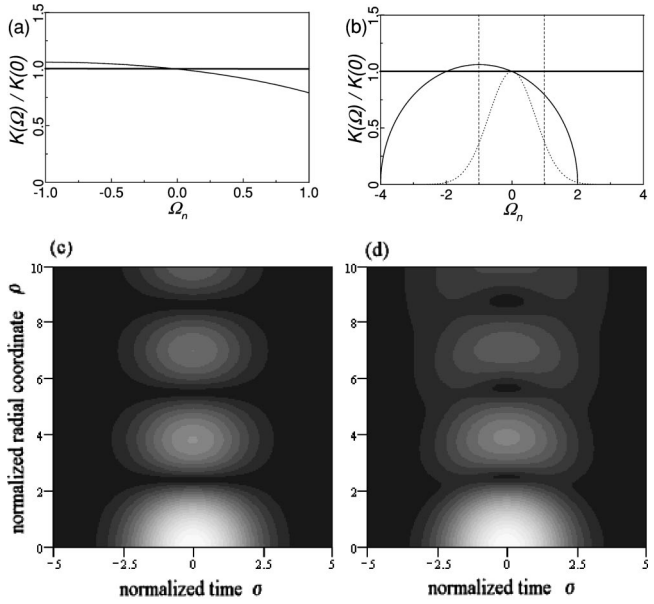

FIG. 5. (a) Dispersion curve within the bandwidth for $|L_p|/|L_w| \to 0$, $|L_p|/|L_d| \to 0$ (thick curve) and for $L_p/L_w = -0.25$, $L_p/L_d = -0.25$ (thin curve). (b) The same as in (a) but also outside the bandwidth of the Gaussian spectrum (in arbitrary units) $\hat{f}(\Omega) = \exp[-(\Omega/\Delta\Omega)^2]$. (c) and (d) Gray-scale plots of the amplitude $|\Phi_{\alpha,\beta}|$ of (c) the PBB of Eq. (21) with spectrum $\hat{f}(\Omega) = \exp \times[-(\Omega/\Delta\Omega)^2]$ (i.e., $f(\tau) \propto \exp[-(2\Delta\Omega\tau)^2]$) and of (d) the mode with $L_p/L_w = -0.25$, $L_p/L_d = -0.25$ and same spectrum as in (c), numerically calculated from Eq. (8). Normalized coordinates are $\sigma = (\tau + \alpha z)\Delta\Omega$, $\rho = r/r_0$, with $r_0 = (2k_0\beta)^{-1/2}$.

Figure 5(c) shows the prototype PBB of this kind of wave mode [Eq. (21)] with a Gaussian spectrum $\hat{f}(\Omega)$ — that is, the limiting case $|L_p/L_w| = 0$, $|L_p/L_d| = 0$—or the horizontal thick lines of Figs. 5(a) and 5(b). In Fig. 5(d) we show, for comparison, the wave mode with $|L_p/L_w| = 0.25$, $|L_p/L_d| = 0.25$ and with the same Gaussian spectrum, obtained numerically from Eq. (8). We see that the wave mode preserves a spatiotemporal structure similar to that of the prototype PBB of Fig. 5(c), even if $|L_p|$ is not much smaller, but simply smaller than $|L_w|$ and $|L_d|$. Small differences can be understood as incipient focus wave mode and O-wave-type behavior, as described in the following sections.

B. Group-velocity-mismatch-dominated case: Envelope focus wave modes

The case $|L_w| \ll |L_p|, |L_d|$ leads to a new kind of wave mode that has not been reported. The dispersion curve within the bandwidth is now of the form of the horizontal parabola $K(\Omega) \simeq 2(k_0 L_w^{-1}\Omega_n)^{1/2}$ with vertex at $\Omega = 0$ or

$$K(\Omega) \simeq \sqrt{2k_0\alpha\Omega} \tag{22}$$

[see Fig. 6(a)], regardless of whether material dispersion is normal [as in Fig. 6(b)] or anomalous. For modes with superluminal group velocity ($\alpha > 0$), the horizontal parabola is right handed [as in Figs. 6(a) and 6(b)], and left handed for subluminal modes ($\alpha < 0$). Independently of the group veloc-

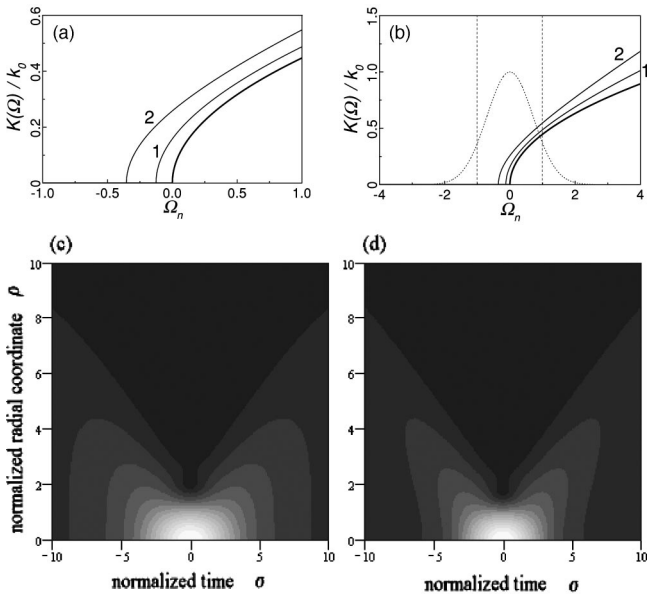

FIG. 6. (a) Dispersion curve within the bandwidth for $L_w=10/k_0$, $L_w/L_p\to 0$, $L_w/L_d\to 0$ (thick curve), for $L_w=10/k_0$, $L_w/L_p=1/8$, $L_w/L_d=1/8$ (thin curve, label 1), and for $L_w=10k_0$, $L_w/L_p=1/3$, $L_w/L_d=1/3$ (thin curve, label 2). (b) The same as in (a) but also outside the bandwidth of the Gaussian spectrum (in arbitrary units) $\hat{f}(\Omega)=\exp[-(\Omega/\Delta\Omega)^2]$. (c) and (d) Gray-scale plots of the amplitude $|\Phi_{\alpha,\beta}|$ of (c) the prototype eFWM [thick dispersion curve in (a)] with spectrum $\hat{f}(\Omega)=\exp[-(\Omega/\Delta\Omega)^2]$ and of (d) the mode with $L_w/L_p=1/3$, $L_w/L_d=1/3$ [thin dispersion curve 2 in (a)], numerically calculated from Eq. (8). Normalized coordinates are $\sigma=(\tau+\alpha z)\Delta\Omega$, $\rho=r/r_0$, with $r_0=(2/k_0\Delta\Omega|\alpha|)^{1/2}$.

ity, phase velocity can be superluminal ($\beta>0$) or subluminal ($\beta<0$). In any case, their spatiotemporal form can be approached by Eq. (8) with $K(\Omega)$ given by Eq. (22). Moreover, with the two-sided exponential spectrum $\hat{f}(\Omega)=(2\pi/\Delta\Omega)\exp(-|\Omega|/\Delta\Omega)$, Eq. (8) yields

$$\Phi_{\alpha,\beta}(r,\tau+\alpha z)\simeq\frac{-i\tau_0}{\tau+\alpha z-i\tau_0}\exp\left[\frac{ik_0|\alpha|r^2}{2(\tau+\alpha z-i\tau_0)}\right] \tag{23}$$

for superluminal modes ($\alpha>0$), and the complex conjugate of the right-hand side of Eq. (23) for subluminal modes ($\alpha<0$). In Eq. (23), $\tau_0\equiv(\Delta\Omega)^{-1}$ characterizes the mode duration. The mode spot size at pulse center ($\tau+\alpha z=0$) can be characterized by $r_0=(2/k_0\Delta\Omega|\alpha|)^{1/2}$.

The functional form of the reduced envelope in Eq. (23) is similar to the fundamental Brittigham-Ziolkowski focus wave mode (FWM) [22,23] and, as such, will be called the envelope focus wave mode (eFWM). There are, however, important physical differences between them, which can be understood for the respective expressions of the complete fields E of both kinds of waves—namely,

$$E_{\alpha,\beta}(r,z,t)\simeq\frac{-i\tau_0}{\tau+\alpha z-i\tau_0}\exp\left[\frac{ik_0|\alpha|r^2}{2(\tau+\alpha z-i\tau_0)}\right]\times\exp(-i\beta z)\exp(-i\omega_0 t+ik_0 z), \tag{24}$$

for the envelope focus wave mode,

$$E(r,z,t)=\frac{-i\tau_0}{\tau-i\tau_0}\exp\left[\frac{ik_0r^2}{2c(\tau-i\tau_0)}\right]\exp(-i\omega_0 t-ik_0 z), \tag{25}$$

with $k_0=\omega_0/c$, for the fundamental FWM [23]. The fundamental FWM is a localized, stationary *free-space* wave whose envelope propagates at luminal group velocity c, whereas the carrier oscillations backpropagate at the same velocity c. The eFWM is also a stationary, localized wave with the same intensity distribution as the fundamental FWM, but propagates in a *dispersive medium* at slightly superluminal or subluminal group velocity $1/(k_0'-\alpha)$. The carrier oscillations propagate in the same direction at slightly superluminal or subluminal phase velocity $\omega_0/(k_0-\beta)$.

Figure 6(c) shows the prototype eFWM of this kind of wave mode, obtained from numerical integration of Eq. (8) with the approximate dispersion curve $K(\Omega)=\sqrt{2k_0\alpha\Omega}$ [thick curves in Figs. 6(a) and 6(b)] — i.e., in the limiting case $|L_w/L_p|=0$, $|L_w/L_d|=0$) — and a Gaussian spectrum. To pursue the validity of the model eFWM to describe this kind of wave mode, we have also evaluated the wave mode field in some nonlimiting cases with the same Gaussian spectrum. For $|L_w/L_p|=1/8$, $|L_w/L_d|=1/8$ [thin curves in Figs. 6(a) and 6(b), label 1], the mode is nearly undistinguishable from the prototype eFWM, despite the dispersion curve differing significantly from the limiting one. Even for the relatively large ratios $|L_w/L_p|=1/3$, $|L_w/L_d|=1/3$ [thin curves in Figs. 6(a) and 6(b), label 2], the calculated wave mode [see Fig. 6(d)] exhibits the same eFWM structure, with some incipient eX-wave behavior because of the actual hyperbolic form (not parabolic) of the dispersion curve, as explained in the next section.

C. Group-velocity-dispersion-dominated case: Envelope X- and envelope O-type modes

1. Normal group velocity dispersion: Envelope X waves

We consider finally modes with $|L_d|\ll|L_p|,|L_w|$ or modes of short enough duration, or propagating in a medium with large enough GVD. When material dispersion is normal ($k_0''>0$), the dispersion curve within the bandwidth approaches the X-shaped curve [see Fig. 7(a)]

$$K(\Omega)\simeq\sqrt{k_0k_0''}|\Omega| \tag{26}$$

of the limiting case $|L_d/L_p|,|L_d/L_w|=0$. The actual dispersion curve of a mode may be slightly shifted towards negative frequencies [as in Figs. 7(a) and 7(b), labels 1 and 2] or positive frequencies for modes with superluminal ($\alpha>0$) or subluminal ($\alpha<0$) group velocities, respectively. For modes with superluminal phase velocity ($\beta>0$), $K(\Omega)$ is real everywhere [Fig. 7(b), label 1], but for modes with subluminal phase velocity there is a narrow frequency gap about $\Omega=0$ [Fig. 7(b), label 2]. A prototype wave mode for this case can be obtained by introducing the approximate dispersion curve of Eq. (26) into Eq. (8). With the two-side exponential spectrum $\hat{f}(\Omega)=(2\pi/\Delta\Omega)\exp(-\Omega/\Delta\Omega)$ we obtain

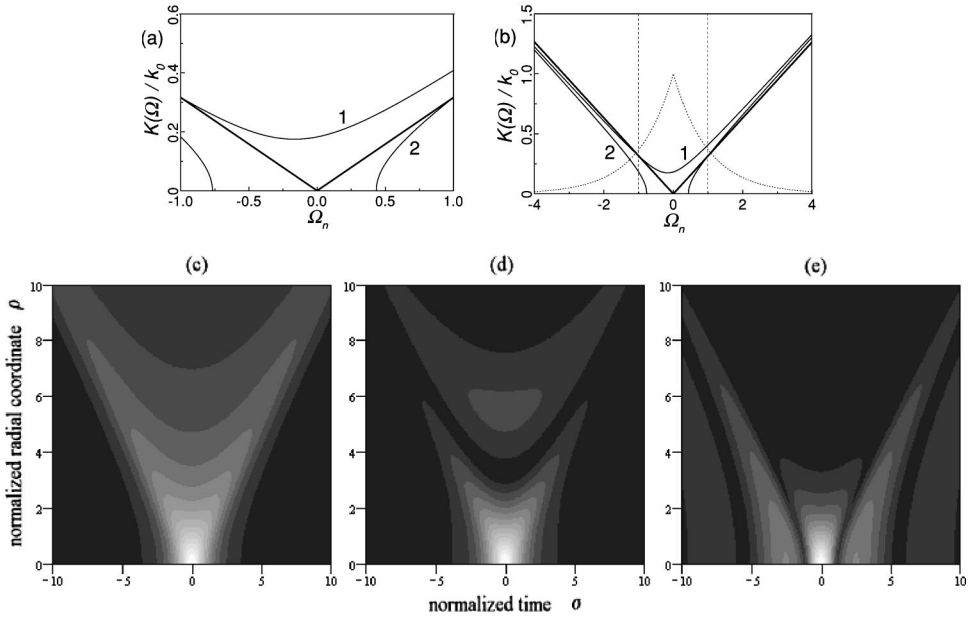

FIG. 7. (a) Dispersion curve within the bandwidth for $L_d=10/k_0$, $L_d/L_p\to 0$, $L_d/L_w\to 0$, with $L_d>0$ (thick curve), for $L_d=10/k_0$, $L_d/L_p=1/6$, $L_d/L_w=1/6$ (thin curve, label 1), and for $L_d=10k_0$, $L_d/L_p=-1/6$, $L_d/L_w=1/6$ (thin line, label 2). (b) The same as in (a) but also outside the bandwidth of the spectrum (in arbitrary units) $\hat{f}(\Omega)=\exp(-|\Omega|/\Delta\Omega)$. (c) – (e) Gray-scale plots of the amplitude $|\Phi_{\alpha,\beta}|$ of (c) the prototype eX [thick dispersion curve in (a)] with exponential spectrum $\hat{f}(\Omega)=\exp[-(\Omega/\Delta\Omega)^2]$ of (d) the mode with $L_d/L_p=1/6$, $L_d/L_w=1/6$ [thin dispersion curve 1 in (a)], and of (e) the mode with $L_d/L_p=-1/6$, $L_d/L_w=1/6$ [thin dispersion curve 2 in (a)]. Normalized coordinates are $\sigma=(\tau+\alpha z)\Delta\Omega$, $\rho=r/r_0$, with $r_0=(k_0k_0''\Delta\Omega^2)^{-1/2}$.

$$\Phi_{\alpha,\beta}(r,\tau+\alpha z)\simeq \mathrm{Re}\left\{\frac{\tau_0}{\sqrt{k_0k_0''r^2+[\tau_0^2+i(\tau+\alpha z)^2]}}\right\}, \tag{27}$$

where $\tau_0\equiv(\Delta\Omega)^{-1}$ measures the pulse duration. Equation (27) is the eX wave recently described in Ref. [13] as an exact, stationary, and localized solution of the paraxial wave equation with luminal phase and group velocities ($\alpha=\beta=0$) in media with normal GVD. The eX wave (27) is understood here as an approximate expression for modes with α,β such that $|L_d/L_p|\ll 1$, $|L_d/L_w|\ll 1$. The spatiotemporal form of the eX wave is shown in Fig. 7(c). For $L_d/L_p=1/6$ ($\beta>0$), $L_d/L_w=1/6$ [thin curves in Figs. 7(a) and 7(b), label 1], the mode retains an X-shaped structure [Fig. 7(d)] despite the dispersion curve differ significantly from the limiting one. Incipient PBB behavior, or radial oscillations, originates from the nearly horizontal dispersion curve in the central part of the spectrum. For $L_d/L_p=-1/6$ ($\beta<0$), $L_d/L_w=1/6$ [thin curves in Figs. 7(a) and 7(b), label 2], the X-shaped mode [Fig. 7(e)] shows instead incipient eFWM behavior (light is within the cone), together with temporal oscillations arising from the frequency gap in the dispersion curve.

2. Anomalous group velocity dispersion: Envelope O waves

When $|L_d|\ll|L_p|,|L_w|$ but GVD is anomalous, the dispersion curve within the bandwidth can be approached by the ellipse centered on $\Omega=0$ [Figs. 8(a) and 8(b), thick curves] given by the expression

$$K(\Omega)\simeq\sqrt{2k_0(\beta-|k_0''|\Omega^2/2)}. \tag{28}$$

Note that the term with β, no matter how small it is, must be retained to reproduce the real-valued part of the dispersion curve. The group velocity of the mode can be slightly subluminal ($\alpha<0$) or superluminal ($\alpha>0$), as in Figs. 8(a) and 8(b) (thin curves), but the phase velocity of these modes is always superluminal ($\beta>0$). An approximate analytical expression for this type of mode can be obtained by introducing the approximate dispersion curve of Eq. (28) into Eq. (8). Under condition $|L_d|\ll|L_p|$, the frequency gap $\Omega_g\simeq\sqrt{2\beta/|k_0''|}$ is much smaller than $\Delta\Omega$, so that the amplitude spectrum $\hat{f}(\Omega)$ can be assumed to take a constant value in the integration domain of integral in Eq. (8), which then yields the expression

$$\Phi_{\alpha,\beta}\simeq\frac{1}{\sqrt{k_0|k_0''|r^2+(\tau+\alpha z)^2}}\times\sin[\sqrt{2\beta/|k_0''|}\sqrt{k_0|k_0''|r^2+(\tau+\alpha z)^2}], \tag{29}$$

of the same form as the O-type impulse response mode in media with anomalous dispersion. Figure 8(c) shows its spatiotemporal form. For comparison, the wave mode with $L_d/L_p=-1/6$, $L_d/L_w=-1/8$ [Fig. 8(a), thin curve] and the two-sided exponential spectrum [Fig. 8(b)] was calculated from Eq. (8), and its O-shaped spatiotemporal form is depicted in Fig. 8(d).

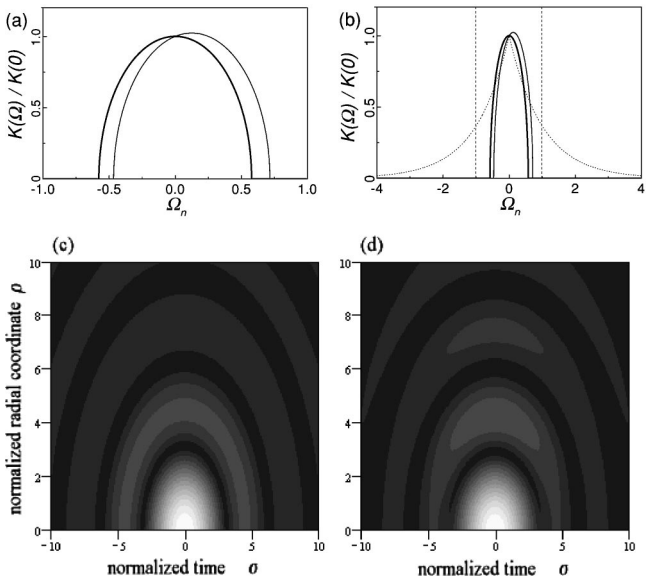

FIG. 8. (a) Dispersion curve within the bandwidth for $|L_d|/|L_p| \to 0$, $|L_d|/|L_w| \to 0$, with $L_d<0$ (thick line), and for $L_d/L_p=-1/6$, $L_d/L_w=-1/8$ (thin curve). (b) The same as in (a) but also outside the bandwidth of the spectrum (in arbitrary units) $\hat{f}(\Omega)=\exp(-|\Omega|/\Delta\Omega)$. (c) Gray-scale plot of the amplitude $|\Phi_{\alpha,\beta}|$ of the eO wave of Eq. (29), (d) of the mode with $L_d/L_p=-1/6$, $L_d/L_w=-1/8$, and the exponential spectrum of (b), numerically calculated from Eq. (8). Normalized coordinates are $\sigma=(\tau+\alpha z)\sqrt{2\beta/|k_0''|}$, $\rho=\sqrt{2k_0\beta}r$.

IV. NONPARAXIAL DESCRIPTIONS OF WAVE MODES

The purpose of this section is to show that the preceding classification of wave modes in dispersive media in terms of the characteristic lengths remains essentially unaltered when performed from the more exact nonparaxial approach, if conditions (2) of quasimonochromaticity and (4) and (5) of quasiluminal group and phase velocities are satisfied.

We consider now the polychromatic Bessel beam

$$E(r,z,t)=\frac{1}{2\pi}\int_{\mathrm{K\ real}} d\omega \hat{f}(\omega-\omega_0)J_0(Kr)\exp(ik_z z)\exp(-i\omega t), \tag{30}$$

where K and k_z must be related by $K=\sqrt{k^2(\omega)-k_z^2}$ for each monochromatic Bessel beam component to satisfy the Helmholtz equation $\Delta\hat{E}+k^2(\omega)\hat{E}=0$. Stationarity of the intensity in some moving reference frame requires the axial propagation constant k_z to be a linear function of frequency [8], a condition that is suitably expressed as

$$k_z(\Omega)=(k_0-\beta)+(k_0'-\alpha)\Omega. \tag{31}$$

Equation (30) can be then rewritten in the form $E(r,z,t)=\Phi_{\alpha,\beta}(r,\tau+\alpha z)\exp(-i\beta z)\exp(-i\omega_0 t+ik_0 z)$, where the reduced envelope is given by the same expression as in the paraxial case—namely,

$$\Phi_{\alpha,\beta}(r,\tau+\alpha z)=\frac{1}{2\pi}\int_{\mathrm{K}(\Omega)\ \mathrm{real}} d\Omega \hat{f}(\Omega)J_0[K(\Omega)r] \times\exp[-i\Omega(\tau+\alpha z)], \tag{32}$$

but with a transversal dispersion relation $K(\Omega)=\sqrt{k^2(\Omega)-k_z^2(\Omega)}$ given now by

$$K(\Omega)=[(2k_0\beta-\beta^2)+2(k_0\alpha+k_0'\beta-\alpha\beta)\Omega + (k_0k_0''+2k_0'\alpha-\alpha^2)\Omega^2]^{1/2} \tag{33}$$

up to second order in dispersion $[k(\Omega)=k_0+k_0'\Omega+k_0''\Omega^2/2]$.

Equations (32) and (33) describe the most general form of nonparaxial wave modes in media with second-order dispersion and contain as particular cases the nonparaxial wave modes in free space described in previous studies. Indeed, in free space ($k_0=\omega_0/c$, $k_0'=1/c$, $k_0''=0$, with c the speed of light in vacuum), Eqs. (32) and (33) yield the general expression (7) of Ref. [24] for free-space FWM's, if the identifications $\alpha=(1-\gamma)/c$ and $\beta=\omega_0\alpha+2\gamma\beta_s$ are made (γ and β_s being the the free parameters defined in Ref. [24]). The case with $\alpha=0$ and $\beta=-2k_0$ yields the original Brittigham's FWM [22,23] with forward propagating envelope and backward propagating carrier oscillations. The choice $\beta=\omega_0\alpha$ leads to the Bessel-X pulse of cone angle $\theta=(2c\alpha)^{1/2}$ or X wave with narrow spectral amplitude centered at an optical frequency, introduced by Saari and Sonajalg in Ref. [16], and demonstrated in Ref. [17].

As for the nonparaxial description of quasiluminal wave modes in dispersive media, we note that the terms β^2, $\alpha\beta$, and α^2 in Eq. (33) can be neglected in comparison with $2k_0\beta$, $k_0\alpha$, and $2k_0'\alpha$, respectively, if conditions (4) and (5) of quasiluminality are satisfied, to obtain the approximate expression

$$K(\Omega)\simeq\sqrt{2(k_0+k_0'\Omega)(\beta+\alpha\Omega)+k_0k_0''\Omega^2} \tag{34}$$

for the nonparaxial dispersion relation of quasiluminal modes. It then follows that the paraxial dispersion curve [Eq. (7)] may significantly differ, under the only condition of quasiluminality, from the nonparaxial one [Eq. (34)]. In fact, it is not difficult to find a set of parameters for which the nonparaxial dispersion curve is, for instance, a vertical hyperbola, whereas the paraxial dispersion curve is a horizontal hyperbola [see Fig. 9(a)]. If the additional condition of quasimonochromaticity is imposed, however, both the paraxial and nonparaxial dispersion curves are essentially the same *within the bandwidth* and, hence, the spatiotemporal structure of the wave mode. Writing $k_0/k_0'\approx\omega_0$ for transparent dispersive materials, we can rewrite Eq. (34) as

$$K(\Omega)\approx\sqrt{2k_0(1+\Omega/\omega_0)(\beta+\alpha\Omega)+k_0k_0''\Omega^2} \tag{35}$$

or, in terms of the characteristic lengths,

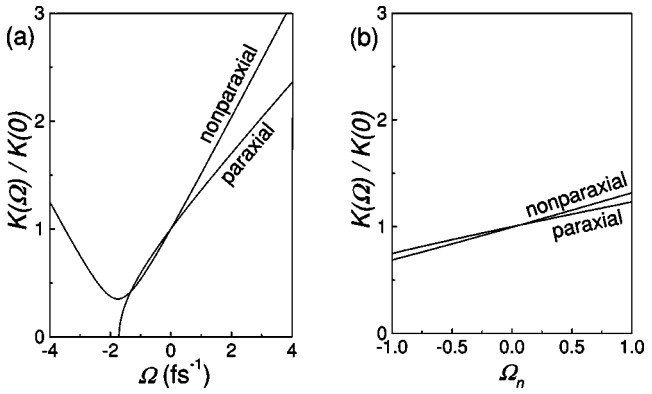

FIG. 9. (a) Paraxial and nonparaxial transversal dispersion curves of the modes of carrier frequency $\omega_0=4$ fs^{-1} with $\alpha=300$ mm^{-1} fs, and $\beta=400$ mm^{-1} in fused silica ($k_0=19\,530$ mm^{-1}, $k_0'=4988$ mm^{-1} fs, and $k_0''=77$ mm^{-1} fs^2). (b) The same as in (a) but only within the bandwidth of the shortest (widest spectrum), single-cycle wave mode ($\Delta\Omega=\omega_0/2\pi$).

$$K(\Omega)\approx\sqrt{2k_0\left[\left(1+\frac{\Delta\Omega}{\omega_0}\Omega_n\right)(L_p^{-1}+L_w^{-1}\Omega_n)+\frac{1}{2}L_d^{-1}\Omega_n^2\right]}. \tag{36}$$

Since $(\Delta\Omega/\omega_0)|\Omega_n|\ll 1$, the nonparaxial dispersion curve within the bandwidth can be approached by the paraxial one—that is, by Eq. (19). This point is illustrated in Fig. 9(b) for the worst possible situation (widest possible bandwidth) of a single-cycle mode ($\Delta\Omega/\omega_0=1/2\pi$). We can then affirm that the description and classification in Sec. III of quasimonochromatic, quasiluminal wave modes in terms of their characteristic lengths is independent of the approach used.

To illustrate the relationship between the paraxial and nonparaxial approaches and the type of results we can expect from the paraxial one, we consider wave modes of any bandwidth $\Delta\Omega$ propagating in normally dispersive media ($k_0''>0$) with

$$\alpha=k_0'-\sqrt{k_0'^2+k_0k_0''}\simeq -k_0k_0''/2k_0', \tag{37}$$

$$\beta=-\frac{k_0(k_0'-\sqrt{k_0'^2+k_0k_0''})}{\sqrt{k_0'^2+k_0k_0''}}\simeq k_0^2k_0''/2k_0'^2, \tag{38}$$

[see Figs. 10(a) and 10(b) for propagation in fused silica], so that the nonparaxial dispersion curve is, from Eq. (34), the (exactly) horizontal straight line

$$K(\Omega)=K\equiv\sqrt{\frac{k_0^3k_0''}{k_0'^2+k_0k_0''}}\simeq\sqrt{\frac{k_0^3k_0''}{k_0'^2}}, \tag{39}$$

and the corresponding nonparaxial wave modes are the dispersion-free, diffraction-free PBB's $\Phi_{\alpha,\beta}(r,\tau+\alpha z)=f(\tau+\alpha z)J_0(Kr)$ studied in Ref. [10]. The approximate equalities in Eqs. (37)–(39) hold for weakly dispersive materials such that $k_0''\ll k_0'^2/k_0$, in which case α and β satisfy conditions (4) and (5) of quasiluminality for the group and phase velocities. As seen in Figs. 10(a) and 10(b), this is the case of fused silica at any visible carrier frequency.

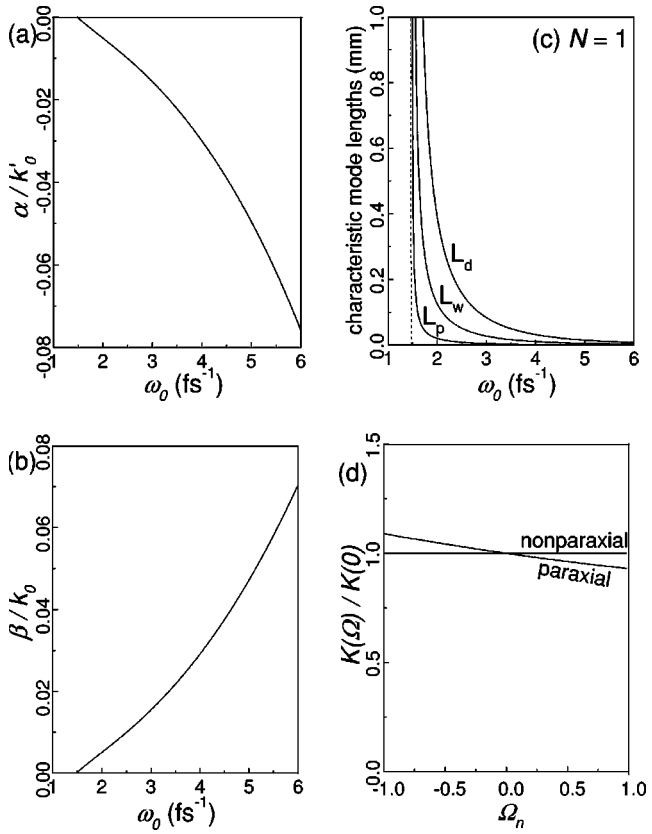

FIG. 10. (a) and (b) Values of α and β from Eqs. (37) and (38) at different carrier frequencies in fused silica, with the refraction index obtained from Ref. [19]. (c) Characteristic lengths for the limiting case of single-cycle modes ($\Delta\Omega=\omega_0/2\pi$), with α and β given by Eqs. (37) and (38) at different frequencies in fused silica. (d) For $\omega_0=2$ fs^{-1} and $\Delta\Omega=\omega_0/2\pi$, comparison between the paraxial and nonparaxial dispersion curves within the bandwidth, given, respectively, by Eqs. (7) and (33).

For these PBB's, it is easy to see that the paraxial and nonparaxial descriptions become undistinguishable, in spite of the apparent drawback that PBB's are no longer exact solutions of the paraxial wave equation in dispersive media [when $k_0''\neq 0$, the paraxial dispersion curve (7) is never a horizontal straight line]. In fact, when $k_0''\ll k_0'^2/k_0$, the relationship $|L_p|\ll|L_w|\ll|L_d|$ is satisfied for any mode bandwidth down to the single-cycle limit [see Fig. 10(c) for the case of fused silica]. Accordingly, these modes are of PBB type; that is, the paraxial dispersion curve within the bandwidth can be approached by an horizontal straight line [see Fig. 10(d) for $\omega_0=2$ fs^{-1} in fused silica]. Finally, the paraxial prototype PBB for these modes is given, from Eq. (21), by $\Phi_{\alpha,\beta}(r,\tau+\alpha z)=f(\tau+\alpha z)J_0(Kr)$, with $K=\sqrt{k_0^3k_0''/k_0'^2}$ — that is, by the same expression as in the nonparaxial approach.

V. CONCLUSIONS

Summarizing, we have described and classified the quasimonochromatic, pulsed versions of Bessel light beams with the property of being localized and remaining stationary (diffraction-free and dispersion-free) during propagation in a

dispersive material with slightly superluminal or subluminal phase and group velocities. As for the wave mode description, we have found the analysis of the transversal dispersion curve $K(\Omega)$, which can be directly related to far field measurements in experiments, to be a useful tool for understanding the spatiotemporal mode structure. Wave modes have been classified into three broad categories: PBB-like, eFWM-like, and eX-like (eO-like) modes, depending on the relative values of their phase and group velocity mismatch with respect to a plane pulse, and defeated GVD, as measured by the mode phase-mismatch length L_p, group-mismatch length L_w, and the dispersion length L_d.

We have verified that the paraxial approach leads to the same results as would be obtained from the more accurate nonparaxial analysis when the conditions of narrow bandwidth (2) and of quasiluminality (4) and (5) are satisfied. All previously reported Bessel beams, X waves, Bessel-X waves, or focus wave modes generated by (linear or nonlinear) optical means satisfy indeed these requirements.

ACKNOWLEDGMENTS

The authors thank G. Valiulis for helpful discussions and acknowledge financial support from MIUR under project Nos. COFIN 01 and FIRB 01.

[1] P. Di Trapani, G. Valiulis, A. Piskarskas, O. Jedrkiewicz, J. Trull, C. Conti, and S. Trillo, Phys. Rev. Lett. **91**, 093904 (2003); see also Phys. Rev. Focus, 4 September 2003 (http://focus.aps.org/story/v12/st7).
[2] O. Jedrkiewicz, J. Trull, G. Valiulis, A. Piskarskas, C. Conti, S. Trillo, and P. Di Trapani, Phys. Rev. E **68**, 026610 (2003).
[3] G. Valiulis, J. Kilius, O. Jedrkiewicz, A. Bramati, S. Minardi, C. Conti, S. Trillo, A. Piskarskas, and P. Di Trapani, *OSA Trends in Optics and Photonics (TOPS)*, QELS 2001, TechnicalDigest, Vol. 57 (Optical Society of America, Washington, D.C., 2001).
[4] C. Conti, S. Trillo, P. Di Trapani, G. Valiulis, A. Piskarskas, O. Jedrkiewicz, and J. Trull, Phys. Rev. Lett. **90**, 170406 (2003).
[5] C. Conti and S. Trillo, Opt. Lett. **28**, 1251 (2003).
[6] C. Conti, Phys. Rev. E **68**, 016606 (2003).
[7] J. Durnin, J. J. Miceli, and J. H. Eberly, Phys. Rev. Lett. **58**, 1499 (1987).
[8] H. Sonajalg and P. Saari, Opt. Lett. **21**, 1162 (1996).
[9] H. Sonajalg, M. Ratsep, and P. Saari, Opt. Lett. **22**, 310 (1997).
[10] M. A. Porras, Opt. Lett. **26**, 1364 (2001).
[11] M. A. Porras, R. Borghi, and M. Santarsiero, Opt. Commun. **206**, 235 (2002).
[12] S. Orlov, A. Piskarskas, and A. Stabinis, Opt. Lett. **27**, 2167 (2002); **27**, 2103 (2002).
[13] M. A. Porras, S. Trillo, and C. Conti, Opt. Lett. **28**, 1090 (2003).
[14] M. A. Porras, G. Valiulis, and P. Di Trapani, Phys. Rev. E **68**, 016613 (2003).
[15] J. Lu and J. F. Greenleaf, IEEE Trans. Ultrason. Ferroelectr. Freq. Control **37**, 438 (1990).
[16] P. Saari and H. Sonajalg, Laser Phys. **7**, 32 (1997).
[17] P. Saari and K. Reivelt, Phys. Rev. Lett. **79**, 4135 (1997).
[18] G. Valiulis (unpublished).
[19] See, for instance, *Handbook of Optics*, 2nd ed. (McGraw-Hill, New York, 1995), Vol. II.
[20] See, for instance, A. Sommerfeld, *Partial Differential Equations in Physics* (Academic, New York, 1949), p. 36.
[21] I. S. Gradshteyn and I. M. Ryzhik, *Table of Integrals, Series and Products* (Academic, New York, 1965).
[22] Brittingham J. Appl. Phys. **54**, 1179 (1983).
[23] R. W. Ziolkowski, Phys. Rev. A **44**, 3960 (1991).
[24] K. Reivelt and P. Saari, J. Opt. Soc. Am. A **17**, 1785 (2000); Phys. Rev. E **65**, 046622 (2002).